

# Polarimetry of $\gamma$ -Rays Converting to $e^+e^-$ Pairs with Silicon-Pixel-Based Telescopes

D. Bernard<sup>a,\*</sup>

<sup>a</sup>LLR, Ecole Polytechnique, CNRS/IN2P3, 91128 Palaiseau, France

## Abstract

There are serious prospects that the next  $\gamma$ -ray space mission could use a telescope based on silicon pixel detectors. I characterize the potential of such active targets for polarimetry with gamma-ray conversions to pairs and find it excellent both in terms of selection efficiency and of effective polarization asymmetry.

**Keywords:** gamma rays, pair conversion, polarization, polarimeter, silicon pixel detector

## 1. Introduction

Efficient measurements of the high-energy  $\gamma$ -ray polarization are eagerly awaited as an additional observable would bring insight on the processes at work in the  $\gamma$  emission of cosmic sources such as pulsars [1, 2] or blazars [3].

Even though various experimental schemes to achieve the measurement of the fraction and of the direction of the linear polarization of a photon beam have been designed and have been characterized successfully by the analysis of simulated data and / or of data collected with a polarimeter prototype on a polarized  $\gamma$ -ray beam [4–6], no such polarimeter has ever been used on a space mission and therefore no polarimetry data of cosmic sources in the MeV energy range is available to date.

Polarimetry is performed by an analysis of the distribution of an azimuthal angle,  $\varphi$ , that measures the orientation of the final state in a plane orthogonal to the direction of the incoming photon (see, e.g., eq. (1) of [7]). In the presence of  $\varphi$  angular resolution, the effective polarization asymmetry,  $A$  is smaller than the theoretical value,  $A_{\text{QED}}$ , by a dilution factor  $D \equiv A/A_{\text{QED}}$ . One of the main issues is the multiple scattering of the electron and of the positron in their way through the detector, that makes the measurement of the azimuthal angle of the pair extremely challenging. In the approximation of a value of the pair opening angle equal to the most probable value of the distribution of that angle, it was demonstrated [8–10] that the dilution factor,  $D$ , inflicted to the polarization asymmetry,  $A$ , varies like  $D = \exp(-2\sigma_0^2 x/X_0)$  with  $\sigma_0 \approx 24$  rad,  $x$  and  $X_0$  the thickness and the radiation length of the scatterer, respectively. So for a photon incident normal to and converting at the top of a 400  $\mu\text{m}$  thick silicon wafer, for example,  $D \approx 0.007$ , an extremely small value. It was believed, therefore, that even before the leptons exited the conversion wafer, most of the azimuthal information was already lost.

This situation led polarimeter designers to extreme decisions, such as the use of a 100  $\mu\text{m}$ -thick carbon converter [4], the use

of an emulsion active target with a single-grain localization precision of 60 nm [5], or of a low-density (gas) high-precision active target such as a time projection chamber (TPC) [6].

A simulation [11] using an event generator that samples the full, 5D, polarized, Bethe-Heitler differential cross section [12] showed, however, that the decrease of the dilution at high thicknesses is milder than that predicted by [8–10], see Fig. 17 of [11], as a number of high-opening-angle events (see Fig. 3 of [13]) still contribute to the sensitivity: there was hope.

An estimate of the performance of a silicon-strip-detector (SSD) / tungsten-foil active target such as the Large Area Telescope (LAT) on the *Fermi* mission [14] was obtained from the analysis of data simulated with a custom-made software and based on a simplified version of the LAT tracker, with a dedicated event reconstruction method [7]. It showed that the effective value of the polarization asymmetry,  $A$ , peaks at the small value of 0.02 at a couple of hundred of MeV (Fig. 21 of [7]). This value of  $A$  is approximately one order of magnitude lower than the QED value (that is, a dilution factor of  $D \approx 0.1$ ).

The variation of  $A_{\text{QED}}$  with photon energy can be found in Fig. 3 of [15]; A high-energy asymptotic expression that is valid down to  $\approx 20$  MeV was obtained by [16] (See also eq. (14) of [17]).

In that situation, a sensitive measurement needs a long exposure on a bright source in the MeV energy range. A study is in progress for the Vela pulsar, that uses the full software package of the *Fermi*-LAT Collaboration [18, 19] with a simulation using an event generation [15, 17, 20] that samples the polarized Bethe-Heitler differential cross-section [12], and with a dedicated event reconstruction. The precision,  $\sigma_P$ , of the measurement of the polarization fraction,  $P$ , on the 15 years of data collected by the LAT, was estimated to be of about 0.15 [7]. Preliminary results obtained from the analysis of simulated data [21] confirm the estimate of the mock-up study [7].

The LAT has been surveying the  $\gamma$ -ray sky from 30 MeV to over 300 GeV, an energy range covering more than four orders of magnitude, since 2008: it is just time to plan a successor mission. Also, between a couple of hundred keV, below which existing Compton telescopes are quite efficient, and a

\*Tel 33 1 6933 5534

Email address: denis.bernard at in2p3.fr (D. Bernard)

couple of hundred MeV, above which the effective area of the LAT is plateauing [22], lies a “sensitivity-gap” for which precise measurements of  $\gamma$ -ray sources are sparse. Several projects are being developed, such as ASTROGAM [23] and AMEGO [24], that in contrast to the LAT do not include tungsten converter foils, so the efficiency and the angular resolution for pair-conversion events at very low-energies is improved. Also, in contrast with the LAT for which each detection layer includes a pair of single-sided silicon-strip detectors, these projects use layers consisting of a single double-sided silicon-strip detector, so that both transverse coordinates ( $x$  and  $y$ ) of low-energy electrons can be measured in the same wafer, enabling an efficient detection of Compton scattering events.

As the sensitivity of the LAT to polarimetry was found to be, to a large extent, originating from conversions in the silicon part of a detection layer (i.e., not in the tungsten foil) [7], as most of the sensitivity of the LAT was found to originate from conversions in the “front” part of the tracker, for which the tungsten foils are thinner, all detectors (LAT, ASTROGAM, AMEGO) can be considered to be “thin” detectors. This implies that the photon conversion probability is much smaller than unity and the effective area is proportional to the sensitive mass ( $28 \text{ cm}^2/\text{kg}$  for 100 MeV photon conversions to pairs on silicon with 100 % efficiency and exposure [25]).

As the silicon mass of the three detectors are similar, as the leptons undergo less multiple scattering in active targets without tungsten foils, and as ASTROGAM and AMEGO are sensitive to pair conversions at lower energies, for which the fluxes from cosmic sources are larger, it can be expected that the polarimetry performance of the projects be better than that of the LAT – even taking into account the different values of the geometrical parameters of the detector.

Recently AMEGO-X, a modified design of AMEGO, has been proposed with silicon pixel detectors in place of silicon strip detectors, with the goal of lowering the capacitance of each segment and therefore to enable the detection of lower energy Compton scattering events [26–29]. The limitation of the available electrical power on a space mission has long hindered the use of pixel-detector active targets for high-effective area  $\gamma$ -ray astronomy; a way out was found by the use of the low-power Complementary Metal Oxide Semiconductor (CMOS) technology AstroPix chip recently developed [26, 29].

In this paper I study the polarimetry performance of telescopes using a pixel-based active target. I first examine the performance of the proposed AMEGO-X set-up [26], after which I explore part of the parameter space, the wafer thickness, in particular. Historically double-sided silicon-strip detectors were designed with a thickness of  $300 \mu\text{m}$ , [30, 31] while  $\gamma$ -ray telescopes use thicker wafers ( $400 \mu\text{m}$  single-sided SSDs for the LAT [32],  $500 \mu\text{m}$  for ASTROGAM [23] and AMEGO [24]) and while high-energy physicists (HEP) are developing thinner and thinner pixel detectors, demonstrated at  $50 \mu\text{m}$  and aiming down to  $20 - 40 \mu\text{m}$  [33].

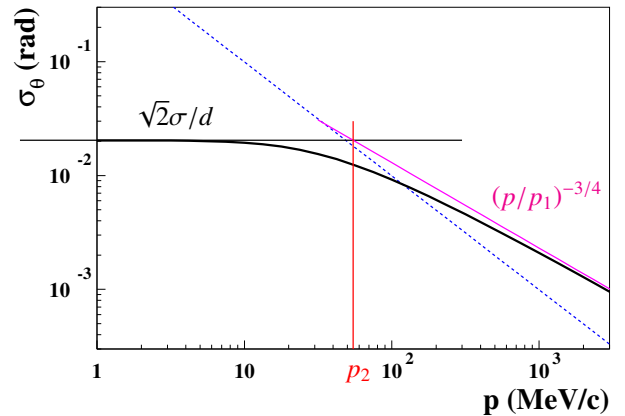


Figure 1: Single-track polar-angle resolution for a  $\gamma$ -ray conversion at the bottom of a wafer, as a function of track momentum. The thick curve is the exact solution (eq. (1) of [37]). The horizontal line is the low-momentum, “coarse detector” asymptote. The inclined line is the high-momentum, “homogeneous detector”, asymptote. The vertical line shows the limit between both ranges, for  $p = p_2$ . The dashed line shows the RMS multiple scattering angle undergone through a full wafer.

## 2. Method

This study is performed with similar tools and in a similar way as my previous work [7].

The detector consists of a number of infinite planes filling the “lower” half space ( $z < 0$ ), irradiated from photons that originate from a cosmic source located “above” the detector. As the selection efficiency and the polarization asymmetry are observed to decrease strongly at large incident angle with the detector boresight,  $\theta$ , events are generated within  $\cos \theta > 0.25$ . The orbits of the telescope and the variation of its attitude are supposed to lead to an isotropic exposure in the detector frame. The number of planes is large enough that all photons convert. Pair-conversion event selection and primary Compton-scattering event rejection are performed from the Monte Carlo information. The propagation and the interactions of the electrons, of the positrons and of the photons in the tracker are simulated with EGS5 [34].

Wafers are of thickness  $e = 500 \mu\text{m}$  and spaced at a distance  $d = 1 \text{ cm}$ , a geometry that corresponds to the detector described in [26]. Pixels are defined by a 2D grid of size  $p = 500 \mu\text{m}$  [26], with the “center” of the detector, ( $x = 0, y = 0$ ), located at the center of a pixel. The passive material on the active area of silicon, expected to amount to  $< 5\%$  [26], is neglected.

For each event, pixels having received a strictly positive amount of energy are recorded. No discriminating threshold is applied as pixels are used to allow the detection of keV energy depositions. Recorded pixels having a side in common are grouped into clusters and the position of the track at its crossing of that particular wafer is defined as the geometric barycenter of the position of the center of the pixels associated to the cluster (using the barycenter of the energies deposited in each pixel yields similar results).

Tracking in the presence of detector position resolution and

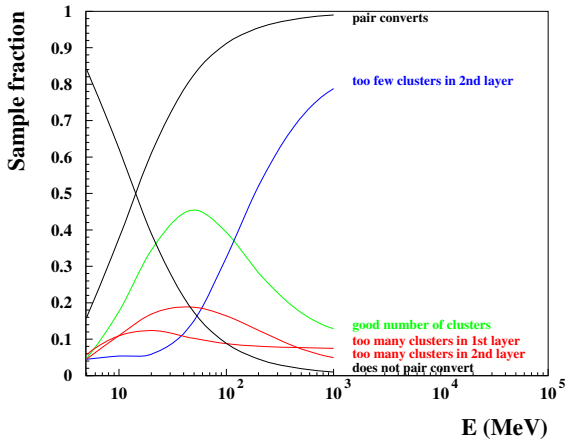


Figure 2: Event fractions as a function of incident photon energy.

of multiple scattering is usually performed in an optimal way using a Kalman filter-based fit [35]. In the case of the LAT, it was shown that over most of the energy range for which the detector has some sensitivity to polarimetry, the polar angle angular resolution of such a fit (neglecting the energy loss of the leptons in their way through the layers), is asymptotically (at low momentum) equal to the angular resolution obtained from measuring the angle simply from the track position in the conversion layer and in the next layer. Hence a Kalman filter was not used [7].

The single-track polar-angle resolution obtained from an optimal fit such as a Kalman-filter fit, for a  $\gamma$ -ray conversion at the bottom of a wafer, was studied in [36]. The R.M.S value is given by eq. (1) of [37], is drawn as the thick curve of Fig. 1 and shows two asymptotes:

- at low track momenta, the angular resolution is  $\sigma_\theta \approx \sqrt{2}\sigma/d$ , that is, the track direction is simply obtained from its positions in the conversion layer and in the next layer ( $\sigma$  is the single-wafer space resolution, here estimated to be equal to  $p/\sqrt{12}$ );
- at higher momenta, the power of the Kalman filter kicks in, additional layers contribute to the measurement, and the angular resolution improves (with respect to  $\sigma_\theta \approx \sqrt{2}\sigma/d$ ), to tend asymptotically to the homogeneous-detector value [11]  $\sigma_\theta \approx (p/p_1)^{-3/4}$ , where the “characteristic” momentum  $p_1$  of the detector is

$$p_1 = p_0 \left( \frac{2\sigma}{d} \right)^{1/3} \left( \frac{e}{X_0} \right)^{1/2}. \quad (1)$$

$p$  is the track momentum and  $p_0 = 13.6 \text{ MeV}/c$  is the multiple scattering constant. The limit between the low- and the high-momentum ranges can be defined by the crossing of the two asymptotes

$$p_2 = p_0 \sqrt{\frac{e}{X_0}} \frac{d}{2^{1/3}\sigma}, \quad (2)$$

that is, for the detector parameters considered in the present study,  $p_2 \approx 55 \text{ MeV}/c$ . For a conversion within a layer, the contribution of multiple scattering within the layer, must be considered in addition (shown as a dashed line in Fig. 1).

As was done for the LAT study [7], only cluster configurations with one cluster per primary track and no additional background noise are used. In the case of the present study, this corresponds to one cluster in the conversion wafer and to two clusters in the next wafer.

The directions of the leptons in the sky frame are calculated from their directions in the detector frame, after which the azimuthal angle of the event,  $\varphi$ , is calculated as the average (the so-called “bissectrix” [38]) of the azimuthal angles of the electron and of the positron.

For event samples simulated with fully polarized photons ( $P = 1$ ) and  $\varphi_0 = 0$ , the polarization asymmetry is computed from the moment of the “optimal” weight  $w = 2 \cos 2\varphi$  ([11] and references therein)<sup>1</sup>.

### 3. Results

Samples of  $10^7$  mono-energetic fully polarized photons from a cosmic source with isotropic exposure within  $\cos \theta > 0.25$  are simulated.

The variation of the fraction of events that are relevant to this analysis (good, too few, too large number of clusters) is presented in Fig. 2. At low energies, a large fraction of events are lost due to Compton scattering, while at high energies, most events are lost because the two tracks create only one cluster in the 2nd layer. Losses due to too many clusters in the 2nd layer are also significant.

The performances of our mock-up polarimeter are presented in Fig. 3.

- (Plot a), the event selection efficiency,  $\epsilon$ , is peaking at  $\epsilon \approx 0.45$  for  $E \approx 50 \text{ MeV}$  (the efficiency is larger close to the zenith of the detector, small  $\theta$ , large  $\cos \theta$  (plot d)).
- (Plot b) the effective polarization asymmetry,  $A$ , is plateauing at  $A \approx 0.09$  (i.e., a dilution factor of about 1/3 at 10 MeV, for which  $A_{\text{QED}} \approx 0.27$  [15]) at very low energies, and then decreases, to reach  $A \approx 0$  at  $E = 1 \text{ GeV}$ .

The most probable pair opening angle distribution is peaking at  $1.6 \text{ rad} \cdot \text{MeV}/E$ , [13], that is, at 1.6 mrad for  $E = 1 \text{ GeV}$ , while the characteristic sampling angle of the detector,  $p/d$ , is equal to the much larger value of 50 mrad (the so-called critical energy,  $E_c$ , for which these two angles are equal [7], is equal to 32 MeV for the detector considered here). 1 GeV photons that converted and that were detected with such a large opening angle that they managed to create two separate clusters in the next wafer most likely underwent a large multiple scattering deflection, hence the blurring of the azimuthal information and the small resulting polarization asymmetry.

<sup>1</sup>In case the polarization angle of the incoming radiation is unknown, a combination of sine and cosine would be used [39].

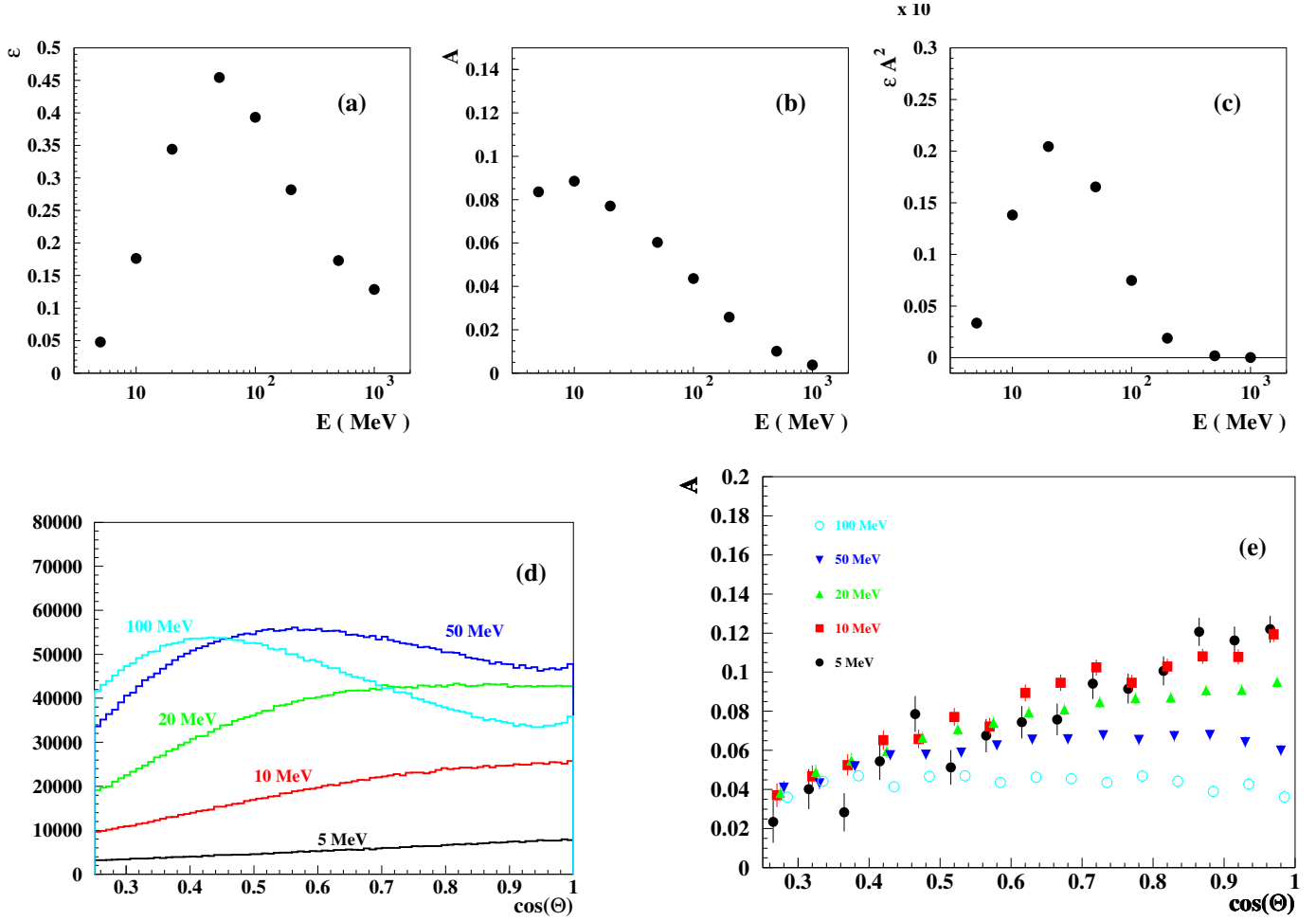


Figure 3: Simulation of samples of  $10^7$  mono-energetic fully polarized photons from a cosmic source with isotropic exposure within  $\cos\theta > 0.25$ , detected in a simplified version of the pixel detector telescope described in [26]. (a) Selection efficiency,  $\epsilon$ , as a function of incident photon energy,  $E$ . (b) Effective polarization asymmetry,  $A$ , as a function of incident photon energy. (c) Figure of merit,  $\epsilon \times A^2$ , as a function of incident photon energy. (d) Incident photon  $\cos\theta$  distributions for selected events, for several photon energies. (e) Effective polarization asymmetry as a function of incident photon  $\cos\theta$  for several photon energies. Small horizontal shifts have been applied to improve readability.

- (Plot c), the figure of merit for polarimetry,  $\epsilon \times A^2$  (see, eg., the discussion in Sects. 12 and 13 of [7]) is peaking at  $E \approx 20$  MeV and is sizeable mainly between 10 and 100 MeV.
- The effective polarization asymmetry,  $A$ , is obviously larger for photon originating from the zenith of the detector, (Plot e) and is plateauing at high  $\cos\theta$  for high energies.

Most of the sensitivity lies in the energy range 10 – 100 MeV, but keep in mind that this analysis is using a sub-optimal tracking for track momentum  $p > p_2 \approx 55$  MeV/c, that is approximately for  $E > 110$  MeV.

I now examine the variation of the performance with the values of the detector parameters.

### Wafer Thickness

Increasing the wafer thickness, all other geometrical param-

eters being kept unchanged, obviously increases the sensitive (silicon) mass and therefore the effective area of the telescope. That main effect is not what I aim to study here, so I generated event samples simulated with various wafer thicknesses, all samples with the same number of generated events of  $10^7$ , which corresponds, for these “thin” active targets, to detectors having the same silicon mass.

The residual variation of the performance for polarimetry is presented in Fig. 4. The selection efficiency decreases mildly with increasing thickness (plot a), mainly due to an increase of the fraction of events with too large a number of clusters in the 2nd layer, while the polarization asymmetry obviously decreases with increasing thickness due to multiple scattering (plot b), and so does the figure of merit  $\epsilon \times A^2$  (plot c).

### Pixel Size

Decreasing the pixel size obviously improves the selection efficiency at high energies. At low energies on the contrary, it

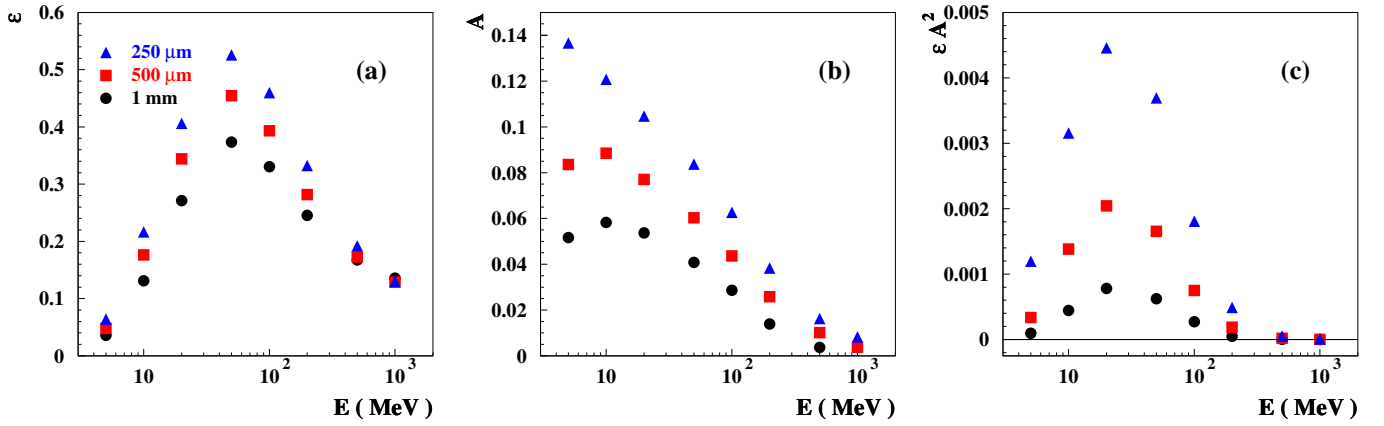


Figure 4: Study of the variation of the performance of the polarimeter with wafer thickness,  $e$  ( $d = 1$  cm,  $p = 500$   $\mu\text{m}$ ). (a) Selection efficiency,  $\epsilon$ , as a function of incident photon energy,  $E$ . (b) Effective polarization asymmetry,  $A$ , as a function of incident photon energy. (c) Figure of merit,  $\epsilon \times A^2$ , as a function of incident photon energy.

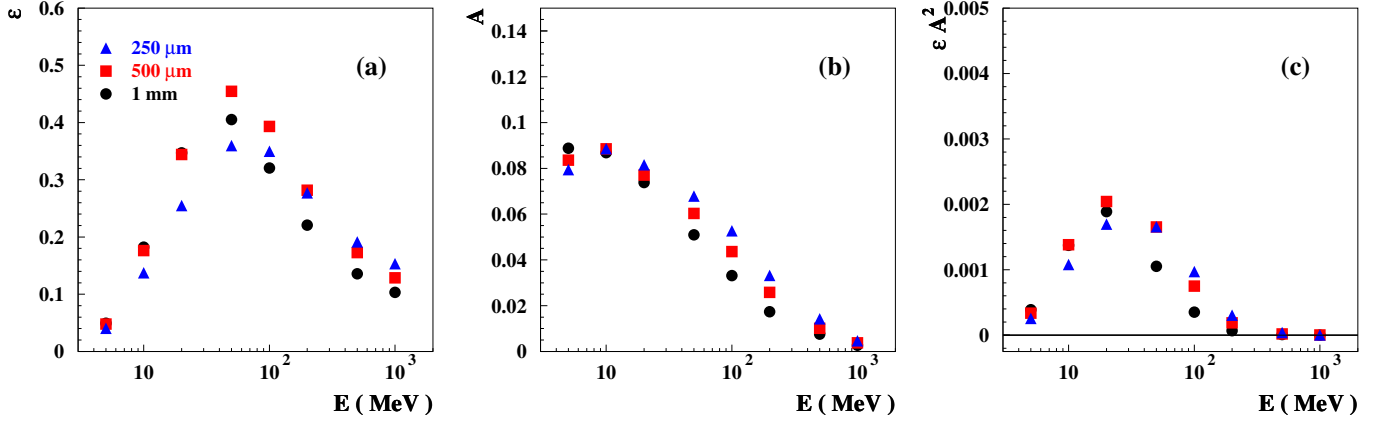


Figure 5: Study of the variation of the performance of the polarimeter with pixel size,  $p$  ( $d = 1$  cm,  $e = 500$   $\mu\text{m}$ ). (a) Selection efficiency,  $\epsilon$ , as a function of incident photon energy,  $E$ . (b) Effective polarization asymmetry,  $A$ , as a function of incident photon energy. (c) Figure of merit,  $\epsilon \times A^2$ , as a function of incident photon energy.

degrades it, due to a larger fraction of events with too many clusters in the 2nd wafer. The polarisation asymmetry is barely affected, something that indicates that the additional contribution of the pixel size to the  $\varphi$  angular resolution is not the dominant factor (Fig. 5).

#### Wafer Spacing

Decreasing the wafer spacing obviously degrades the selection efficiency at high energies, as fewer events have a pair opening angle large enough to induce two separate clusters in the next wafer (Fig. 6). As for the variation of the pixel size, the polarisation asymmetry is barely affected.

#### 4. Polarimeter performance

Given the strong variation of the polarization asymmetry with energy, the polarization fraction is measured with an event

weighting as described in Sect. 12 of [7]. The precision of its measurement,  $\sigma_P$ , is then (eq. (19) of [7])

$$\sigma_P = \sqrt{\frac{2}{\sum_k A_k^2 N_k}}. \quad (3)$$

where  $A_k$  and  $N_k$  are the effective polarization asymmetry and the number of events of energy bin  $k$ , with

$$N_k = \frac{\eta \epsilon_k F_0 \Delta E_k H(E_k) T m}{E_k^2}, \quad (4)$$

for a bright source with spectral index equal to 2, and a differential flux equal to  $F_0/E^2$ ,  $F_0 = 10^{-3}$  MeV/(cm<sup>2</sup>s),  $m$  the detector silicon mass,  $T$  the duration of the data collection,  $H(E_k)$  the total photon attenuation at photon energy  $E_k$  [25],  $\Delta E_k$  the width of energy bin  $k$  and the exposure factor  $\eta = (1 - \cos(\theta_{\text{cut}}))/2 \approx 0.375$ . An overall figure of merit for the

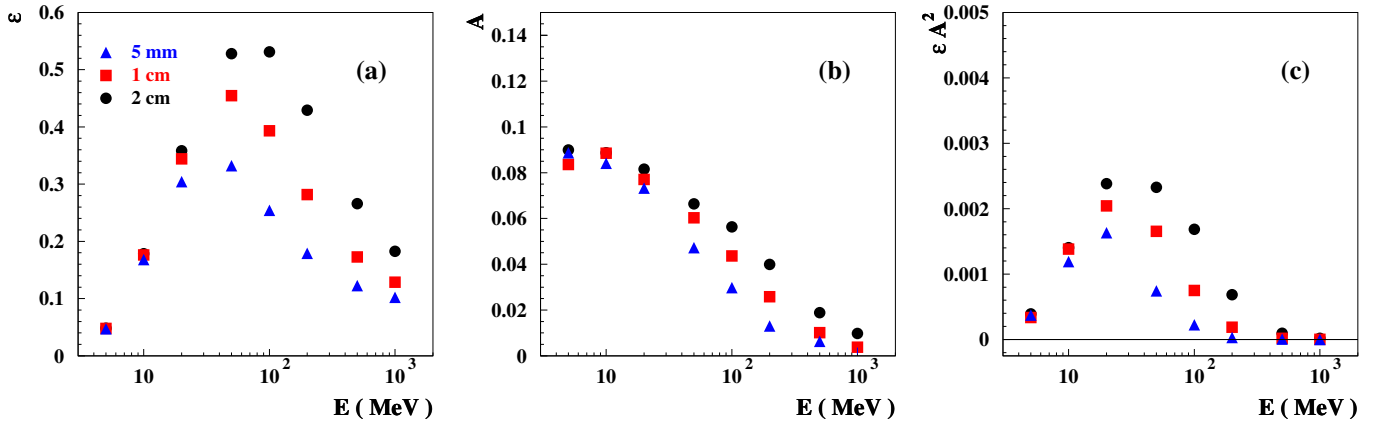


Figure 6: Study of the variation of the performance of the polarimeter with wafer spacing  $d$  ( $e = 500 \mu\text{m}$ ,  $p = 500 \mu\text{m}$ ). (a) Selection efficiency,  $\epsilon$ , as a function of incident photon energy,  $E$ . (b) Effective polarization asymmetry,  $A$ , as a function of incident photon energy. (c) Figure of merit,  $\epsilon \times A^2$ , as a function of incident photon energy.

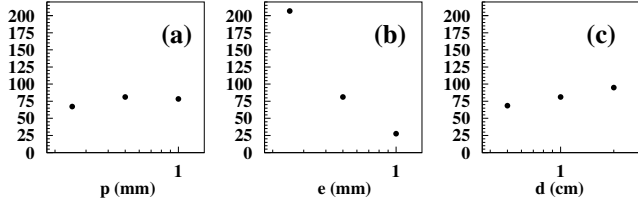


Figure 7: Variation of the performance of the polarimeter, expressed as the value of  $\lambda \equiv \sum_k A_k^2 N_k / (T m)$ , with the values of the detector pixel size (a), wafer thickness (b), and wafer spacing (c).

performance of a given detector configuration can be defined as  $\lambda \equiv \sum_k A_k^2 N_k / (T m)$ .

For the parameter set of this study ( $e = 500 \mu\text{m}$ ,  $d = 1 \text{ cm}$ ,  $p = 500 \mu\text{m}$ ),  $\lambda$  is found to be equal to  $81 \cdot (\text{year} \cdot \text{kg})^{-1}$ , so for a 5 year, 30 kg [28] mission, a precision of  $\sigma_p \approx 0.013$  would be within reach.

The variation of  $\lambda$  with the detector parameter values considered in the previous section is presented in Fig. 7. The wafer thickness is clearly the parameter that determines the overall performance of the polarimeter.

## 5. Conclusion

I have studied the performance of an all-silicon, pixel-based, active target tracker for polarimetry in the pair creation regime. The analysis proved to be much simpler with pixel detectors than that for strip detectors [7]. By comparison with the *Fermi* LAT, the absence of tungsten foils extends the sensitivity range to lower energies, for which the flux of cosmic sources is higher and the pair opening angle is larger. As a result the precision of the polarization fraction that can be expected is improved, even for a smaller silicon sensitive mass and a shorter mission duration. Using pixels (AMEGO-X) instead of strips (AMEGO), with other parameter (wafer thickness, strip pitch / pixel size,

layer spacing) kept unchanged, removes the loss in polarization asymmetry induced for the strip detector by the ambiguity between two photon candidates when two clusters are present in both  $x$  and  $y$  direction. The selection efficiencies and the polarization asymmetries are found to be sizeable. The selection efficiency improves, at high energies, with larger wafer spacing. The polarization asymmetry improves with thinner wafers on the whole energy range. This study indicates that measurements of the polarization fraction of the brightest sources of the MeV  $\gamma$ -ray sky with a precision of several per-cents may be within reach.

## 6. Acknowledgements

I would like to pay tribute to my colleague Berrie Giebels who converted me to polarimetry and who sadly passed away last year.

## References

- [1] A. K. Harding and C. Kalapotharakos, “MeV Pulsars: Modeling Spectra and Polarization,” *PoS IFS* **2017** (2017) 006.
- [2] A. K. Harding and C. Kalapotharakos, “Multiwavelength Polarization of Rotation-Powered Pulsars,” *Astrophys. J.* **840** (2017) 73.
- [3] H. Zhang and M. Böttcher, “X-Ray and Gamma-Ray Polarization in Leptonic and Hadronic Jet Models of Blazars,” *Astrophys. J.* **774** (2013) 18.
- [4] C. de Jager *et al.*, “A Pair Polarimeter for Linearly Polarized High Energy Photons,” *Eur. Phys. J. A* **19** (2004) 275.
- [5] K. Ozaki *et al.*, “Demonstration of polarization sensitivity of emulsion-based pair conversion telescope for cosmic gamma-ray polarimetry,” *Nucl. Instrum. Meth. A* **833** (2016) 165.
- [6] P. Gros *et al.*, “Performance measurement of HARPO: A time projection chamber as a gamma-ray telescope and polarimeter,” *Astropart. Phys.* **97** (2018) 10.
- [7] D. Bernard, “MeV-GeV Polarimetry with  $\gamma \rightarrow e^+e^-$ : Asserting the Performance of Silicon Strip Detectors-Based Telescopes,” *Nucl. Instrum. Meth. A* **1042** (2022), 167462
- [8] S.R. Kel’ner *et al.*, “Methods of measuring linear polarization of gamma quanta”, *Yad. Fiz.* **21** (1975) 604, *Sov. J. Nucl. Phys.* **21**.
- [9] Yu. D. Kotov, “Methods of measurement of gamma-ray polarization”, *Space Science Reviews* **49** (1988) 185.
- [10] Mattox, J. R. *et al.*, “Analysis of the COS B data for evidence of linear polarization of VELA pulsar gamma rays”, *Astrophys. J.* **363** (1990) 270.
- [11] D. Bernard, “Polarimetry of cosmic gamma-ray sources above  $e^+e^-$  pair creation threshold,” *Nucl. Instrum. Meth. A* **729** (2013) 765.
- [12] M. M. May, “On the Polarization of High Energy Bremsstrahlung and of High Energy Pairs”, *Phys. Rev.* **84** (1951) 265.
- [13] H. Olsen, “Opening Angles of Electron-Positron Pairs,” *Phys. Rev.* **131** (1963) 406.
- [14] W. B. Atwood *et al.* [Fermi-LAT Collaboration], “The Large Area Telescope on the Fermi Gamma-ray Space Telescope Mission,” *Astrophys. J.* **697** (2009) 1071.
- [15] I. Semeniouk and D. Bernard, “C++ implementation of Bethe-Heitler, 5D, polarized,  $\gamma \rightarrow e^+e^-$  pair conversion event generator,” *Nucl. Instrum. Meth. A* **936** (2019) 290
- [16] V. F. Boldyshev and Y. .P. Peresunko, “Electron-positron pair photoproduction on electrons and analysis of photon beam polarization,” *Yad. Fiz.* **14** (1971) 1027.
- [17] D. Bernard, “A 5D, polarised, Bethe-Heitler event generator for  $\gamma \rightarrow e^+e^-$  conversion,” *Nucl. Instrum. Meth. A* **899** (2018) 85.
- [18] P. Boinee *et al.* “GLEAM: The GLAST Large Area Telescope Simulation Framework,” [arXiv:astro-ph/0308120 [astro-ph]].
- [19] W. Atwood *et al.* [GLAST LAT], “The full simulation of the GLAST LAT high energy gamma ray telescope,” (Calor 2004), 329
- [20] V. Ivanchenko *et al.* “Geant4 electromagnetic physics progress,” *EPJ Web Conf.* **245** (2020) 02009
- [21] A. Laviron *et al.* [Fermi-LAT], “MeV-GeV polarimetry with the *Fermi-LAT*,” *PoS ICRC2023* (2023) 721
- [22] “Fermi LAT Performance”, Pass 8 Release 3 Version 3, Dec 01, 2021. [https://www.slac.stanford.edu/exp/glast/groups/canda/lat\\_Performance.htm](https://www.slac.stanford.edu/exp/glast/groups/canda/lat_Performance.htm)
- [23] A. De Angelis *et al.* [e-ASTROGAM], “Science with e-ASTROGAM: A space mission for MeV–GeV gamma-ray astrophysics,” *JHEAp* **19** (2018) 1-106
- [24] R. Caputo *et al.* [AMEGO], “All-sky Medium Energy Gamma-ray Observatory: Exploring the Extreme Multimessenger Universe,” (2019) arXiv:1907.07558 [astro-ph.IM]]
- [25] “XCOM: Photon Cross Sections Database, NIST Standard Reference Database 8 (XGAM)”, National Institute of Standards and Technology, nist.gov, 2010.
- [26] I. Brewer *et al.*, “Developing the future of gamma-ray astrophysics with monolithic silicon pixels,” *Nucl. Instrum. Meth. A* **1019** (2021), 165795 [arXiv:2109.13409 [astro-ph.IM]].
- [27] H. Fleischhack, “AMEGO-X: MeV gamma-ray Astronomy in the Multi-messenger Era,” *PoS ICRC2021* (2021), 649, [arXiv:2108.02860 [astro-ph.IM]].
- [28] R. Caputo *et al.*, “The All-sky Medium Energy Gamma-ray Observatory eXplorer (AMEGO-X) Mission Concept,” [arXiv:2208.04990 [astro-ph.IM]].
- [29] A. L. Steinhebel *et al.*, “AstroPix: Novel monolithic active pixel silicon sensors for future gamma-ray telescopes,” [arXiv:2209.02631 [astro-ph.IM]], Contribution to: ISVHECRI 2022
- [30] P. Holl *et al.* “The Aleph Minivertex Detector,” *Nucl. Instrum. Meth. A* **257** (1987), 587
- [31] C. Bozzi *et al.* [BaBar], “The BaBar silicon vertex tracker,” *Nucl. Instrum. Meth. A* **435** (1999), 25
- [32] W. B. Atwood *et al.*, “Design and Initial Tests of the Tracker-Converter of the Gamma-ray Large Area Space Telescope,” *Astropart. Phys.* **28** (2007) 422.
- [33] G. A. Rinella *et al.* [ALICE ITS project], “First demonstration of in-beam performance of bent Monolithic Active Pixel Sensors,” *Nucl. Instrum. Meth. A* **1028** (2022), 166280
- [34] H. Hirayama *et al.*, “The EGS5 code system,” SLAC-R-730, KEK-2005-8, KEK-REPORT-2005-8, version: January 13, 2016.
- [35] R. Frühwirth, “Application of Kalman filtering to track and vertex fitting,” *Nucl. Instrum. Meth. A* **262** (1987) 444.
- [36] M. Frosini and D. Bernard, “Charged particle tracking without magnetic field: optimal measurement of track momentum by a Bayesian analysis of the multiple measurements of deflections due to multiple scattering,” *Nucl. Instrum. Meth. A* **867** (2017) 182.
- [37] D. Bernard, “Performance of the MeV gamma-ray telescopes and polarimeters of the future.  $\gamma \rightarrow e^+e^-$  in silicon-detector active targets,” arXiv:1902.07910 [astro-ph.IM], presented at the 12th INTEGRAL conference and 1st AHEAD Gamma-ray workshop, 11 - 15 Feb. 2019, Geneva.
- [38] P. Gros and D. Bernard, “ $\gamma$ -ray polarimetry with conversions to  $e^+e^-$  pairs: polarization asymmetry and the way to measure it,” *Astropart. Phys.* **88** (2017) 30.
- [39] F. Kislat *et al.*, “Analyzing the data from X-ray polarimeters with Stokes parameters,” *Astropart. Phys.* **68** (2015) 45.